Pergamon

1359-4311(95)00076-3

Applied Thermal Engineering Vol. 16, Nos 8/9, pp. 719–731, 1996

1359-4311/96 $15.00 + 0.00

HORIZONTAL FLOW BOILING OF R22 AND R407C IN A 9.52 MM MICRO-FIN TUBE

Cheng-Shu Kuo* and Chi-chuan Wang†‡

*Department of Mechanical Engineering, National Chiao Tung University, Hsinchu, 300 Taiwan; and †Energy and Research Laboratories, Industrial Technology Research Institute, Hsinchu, 310 Taiwan

(*Received* 22 *October* 1995)

Abstract—The two-phase heat transfer coefficient and pressure drop characteristics of refrigerant R22 and R407C (a mixture of R32/R125/R134a, 23%/25%/52%) in a micro-fin tube with nominal diameter 9.52 mm were presented in this study. Experimental data were taken at an evaporation pressure of 600 kPa. The mass flux was between 100 and 300 kg/m²·s and the heat fluxes were between 6 and 14 kW/m². Experimental data were presented in the form of length-averaged heat transfer coefficients and frictional pressure gradients. The effect of heat flux and mass flux on the heat transfer coefficients were also reported in the present investigation. It is found that the heat transfer coefficients for R407C are considerably lower than R22 (50~80% less), and the pressure drop of R407C is 30~50% lower as compared to R22. Copyright © 1996 Elsevier Science Ltd

Keywords—R407C, heat transfer coefficients, evaporator.

NOMENCLATURE

A_o	outside heat transfer area of the tube (m²)
A_i	nominal inside heat transfer area of the tube (m²)
Cp	specific heat of water (J/kg K)
dP_f	measured two-phase frictional pressure difference (N/m²)
dP_{fl}	frictional pressure difference for liquid flowing alone (N/m²)
$dP_{f,lo}$	frictional pressure difference for total mixture flowing as liquid (N/m²)
D_i	maximum inside diameter of the tube (m)
D_o	nominal outside diameter of the tube (m)
f_i	single-phase friction factor
f_{TP}	two-phase friction factor
G	mass flux (kg/m²·s)
i_{fg}	latent heat of evaporating vapour (J/kg)
L	effective heating length (m)
$LMTD$	log mean temperature difference (K)
$\dot{m}_r$	average mass flow rate of refrigerant (kg/s)
$\dot{m}_{water}$	average mass flow rate of coolant water (kg/s)
P_{sat}	saturation pressure, kPa
ΔP_a	pressure drop due to acceleration (N/m²)
ΔP_f	frictional pressure drop (N/m²)
q	average heat flux (W/m²)
$\dot{Q}$	average heat transfer rate (W)
Re_{eq}	equivalent two-phase Reynolds number
R_w	wall resistance (m²·K/W)
T_{sat}	saturation temperature of the pure refrigerant R22 (K)
T_{bubble}	bubble point temperature of the refrigerant mixture R407C (K)
$T_{bubble,x}$	bubble point temperature evaluated at the local axial concentration during the evaporation process of R407C (K)
$T_{bubble,i}$	bubble point temperature evaluated at the original concentration of R407C (K)
T_w	wall temperature (K)
ΔT	temperature rise on the water coolant (K)
U_o	overall heat transfer coefficient (W/m²·K)
$\bar{v}$	average specific volume (m³/kg)
x	vapour quality
X	Martinelli parameter
Δx	difference of quality

Greek letters

ρ	density of refrigerant (kg/m³)
$\bar{\rho}$	average two-phase density ($1/\bar{v}$) (kg/m³)

‡Author to whom correspondence should be addressed at: D200 ERL/ITRI Bldg. 64, 195~6 Section 4, Chung Hsing Rd., Chutung, 310, Hsinchu, Taiwan.

ϕ^2_l two-phase friction multiplier for liquid flowing alone
μ dynamic viscosity of refrigerant (N·s/m²)

Subscripts
ave average value
bubble based on bubble point temperature
f liquid phase
i inside
in refrigerant inlet condition
o outside
w wall
water water

INTRODUCTION

Numerous augmentation techniques have been suggested for in-tube evaporation heat transfer. Coated, corrugated, fluted and integral tubes along with twisted tapes are used for flow boiling [1]. For refrigeration and air-conditioning applications, the micro-fin tube is widely used. This tube has small fins of triangular cross-section at a helix angle of approximately 8–30°. One of the reasons for the growing popularity of the micro-fin tube is the larger heat transfer enhancement relative to the increased pressure drop. Generally, a 50–100% increase in evaporation and condensation heat transfer coefficient occurs, while only a 20–50% increase in pressure drop was reported for various kinds of refrigerants, including R-113 [2], R-22 [3–6] and R-134a [7]. Although considerable data have been published on the micro-fin tubes, most of the published data are related to the pure refrigerants. As is well known, the most recent revision of the Montreal Protocol at the Copenhagen conference (1992) concluded that R22 will be phased out early next century, and one of the potential substitute candidates of R22, R407C, is a mixture of 23 wt% of R32, 25 wt% of R125 and 52% of R134a. However, experimental data on the most important refrigerant substitute of R22, namely R407C, are very rare at present.

During the past decade, much work has been done toward the understanding of the boiling process with mixtures. Detailed mechanisms of convective evaporation with mixtures were investigated by Ross *et al.* [8]. A unique phenomenon contrary to the pure refrigerant was observed, the wall temperature at the bottom was lower than that at the top, so the heat transfer coefficient at the bottom was higher than at the top. Jung *et al.* [9] investigated horizontal forced convective evaporation with R22, R114 and their mixtures. Their results indicate an early suppression of nucleate boiling for the mixtures. A lot of experiments have been conducted on the investigation of in-tube evaporation of mixtures, as reviewed by Wang and Chato [10], and a chronological listing of relevant references that provide experimental heat transfer data for pool boiling, forced convective boiling and falling-film evaporation of mixtures. Although many efforts have been made to study the heat transfer and friction characteristics for the refrigerant mixtures, most of the existing data, especially with zeotropic mixtures, are very equipment- and refrigerant-specific and generally should not be extrapolated outside the ranges specified and to other refrigerants. Accordingly, the key objective of the present study is to provide heat transfer coefficients and pressure drop data for R407C within a 9.52 mm micro-fin and a smooth tube under practical evaporation conditions.

EXPERIMENTAL APPARATUS

The schematic of the experimental apparatus is depicted in Fig. 1. The test rig was composed of three independent flow loops; namely, a refrigerant loop, a heating water flow loop and a glycol flow loop. The refrigerant loop is an oil-free pump-driven system, which includes a preheater, test section, after condenser, and the refrigerant gear pump with adjustable refrigerant volume, and can provide refrigerant mass fluxes from 50 to 500 kg/m²·s. To ensure the refrigerant was completely condensed before entering the flow measuring device, a subcooler was installed at the exit of the refrigerant pump. Leaving the subcooler, the mass flow rate was measured by a very accurate coriolis mass flow meter with 0.2% precision of the test span. Then, the subcooled refrigerant liquid was heated in the preheater to achieve a prescribed evaporator inlet quality before entering the test section. Then, the refrigerant went into the test section to vaporize. Finally, the two-phase

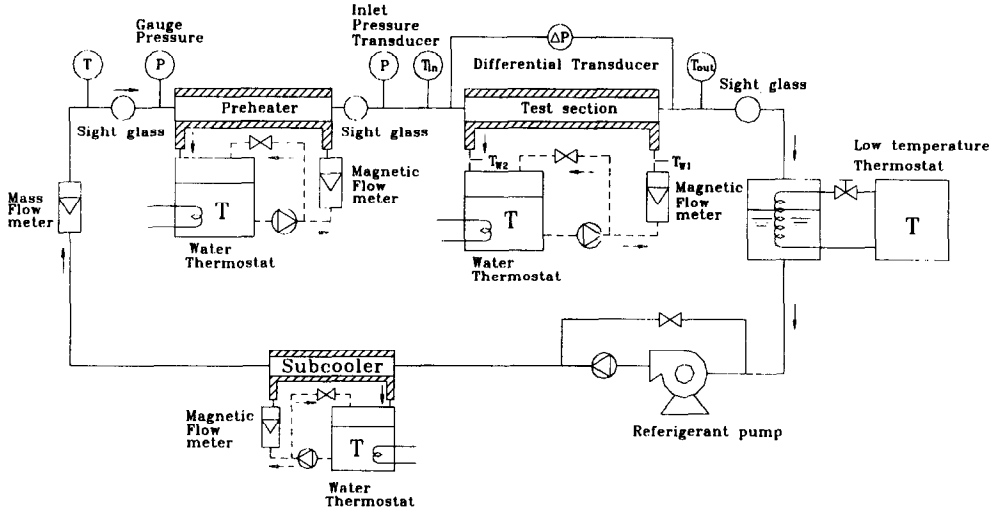

Fig. 1. Schematic diagram of test apparatus.

refrigerant is condensed in a shell-and-coil condenser. Note that an independent low-temperature thermostat using glycol as the working medium with a cooling capacity up to 15 kW was used to condense the refrigerant vapour in the shell-and-coil condenser. The horizontal test section was a double-pipe heat exchanger with effective heat transfer length of 1.3 m. Its detailed configuration can be seen in Fig. 2. A 50-mm-thick rubber insulation was wrapped around the double-pipe heat exchanger to ensure heat loss to the ambient is less than 20 W. As is seen from Fig. 2, inside the double-pipe heat exchanger, water flowed countercurrently in the annulus of the test section, while refrigerant was evaporated inside the test tube. The pressure drop of the refrigerant across the test tube was measured by a differential pressure transducer with 10 Pa precision. Two magnetic flow meters were used to record the flow rates of water in the annulus of the preheater and the test section. These magnetic flow meters were calibrated in advance with a calibrated accuracy of 0.002 l/s. Two absolute pressure transducers were installed at the inlet and exit of the test section with a resolution up to 0.1 kPa. During each experiment, the heat flux in the test section was maintained at a desired constant value. This may be accomplished by simultaneously controlling the inlet temperature and the water flow rate within the annulus. Experiments were conducted using a commercially available 9.52 mm micro-fin tube. For comparison purpose, a smooth tube with identical outside diameter was tested in the present investigation. The geometrical parameters of the test tubes are given in Table 1. Tests were conducted at a 600 kPa evaporation pressure.

All the water and refrigerant temperatures were measured by RTDs (Pt100 Ω) having a calibrated accuracy of 0.05°C The data signals were collected and converted by a data acquisition system

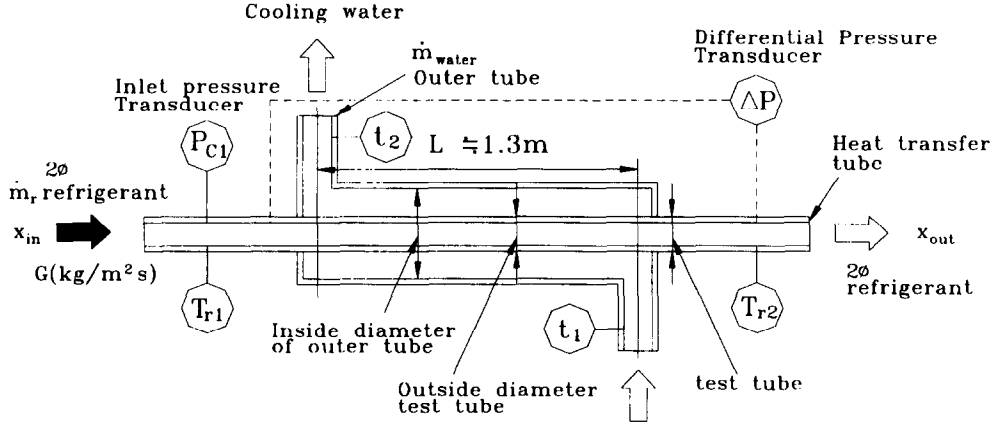

Fig. 2. Details of the test section.

Table 1. Geometrical parameters of test tubes

Tube groove type	Outside diameter OD (mm)	Wall thickness TF (mm)	Fin height H (mm)	Helix angle α	Number of fins N	Inside surface area cm^2/m	Tube length – (mm)
Smooth	9.52	0.8	–	–	–	248	1300
Micro-fin	9.52	0.3	0.20	18	60	440	1300

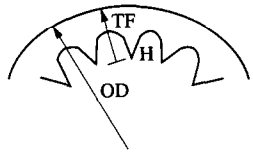

(Hybrid recorder). The data acquisition system then transmitted the converted signals through a GPIB interface to a host computer for further operation. Both the thermodynamic and transport properties of the R407C were evaluated using a computer program [11]. However, the surface tension for R407C is not available by the NIST program. Therefore, the ideal mixing rule was used to obtain the surface tension data for the R407C refrigerant. Table 2 shows the comparison of the thermodynamic and transport properties of the R22 and R407C refrigerants. At the evaporation pressure of 600 kPa, the transport properties of R407C are very similar to R22. The vapour heat capacity of R407C is 13% higher than that of R22 and 10.5% higher than that of R22 in the liquid phase. Uncertainties of the heat transfer coefficients and friction factors reported in the present investigation, following the single-sample analysis proposed by Moffat [12], are tabulated in Table 3.

Table 2. Comparison of thermophysical properties of R22 and R407C

Property	R22	R407C
P_{sat} (kPa)	600	600
T_{sat} (°C)	6.04	1.66
ρ_f (kg/m³)	1262	1246
ρ_g (kg/m³)	25.66	25.03
Cp_f (kJ/kg K)	1.214	1.377
Cp_g (kJ/kg K)	0.7896	0.8722
i_{fg} (kJ/kg)	197.8	215.4
μ_f (10^{-6} N s/m²)	12.03	11.83
μ_g (10^{-6} N s/m²)	207.7	219.6
k_g (mW/m K)	9.7	11.9
k_f (mW/m K)	99.62	102.0

Table 3. Summary of estimated uncertainties

Primary measurements		Derived quantities		
Parameter	Uncertainty	Parameter	Uncertainty G = 100 kg/m² s	Uncertainty G = 300 kg/m² s
m_f	0.3–0.8%	G	1.0%	0.5%
m_{water}	0.5%	Re_i	0.6%	0.6%
ΔP	0.5%	dP/dZ	± 0.8%	± 0.65%
T	0.05°C	h	± 9.4%	± 12.4%

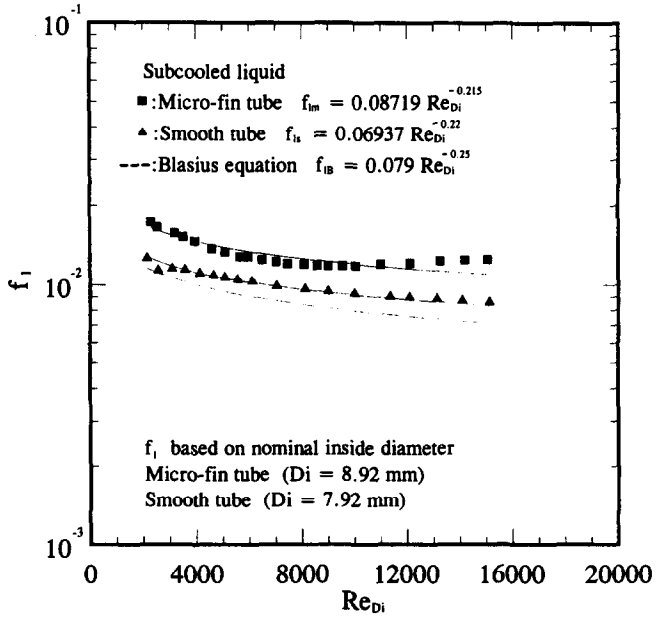

Fig. 3. Subcooled liquid friction factors in smooth and micro-fin tubes.

HEAT TRANSFER DATA REDUCTION

The in-tube heat transfer coefficient can be obtained from the thermal resistance equation:

$$h_o = \frac{1}{\frac{1}{U_o} - R_w A_o - \frac{A_o}{h_i A_i}}, \tag{1}$$

where the overall heat transfer coefficient is given as

$$U_o = \frac{\dot{Q}}{LMTD \times A_o}. \tag{2}$$

For pure refrigerant R22, the saturation temperature, T_{sat}, is used in the calculation of $LMTD$, and the bubble point temperature of R407C is used in the calculation of $LMTD$. Note that the bubble point temperature is based upon the original composition of R407C. In the evaporation of mixtures, the light components are generally more volatile than the less volatile component. Consequently, the mixtures become denuded of the lighter components. Thus, the effective driving potential of the heat transfer for the mixtures, $T_w - T_{bubble,x}$, becomes less than the original driving potential, $T_w - T_{bubble,i}$. This implies the use of the driving potential, $T_w - T_{bubble,i}$, may result in smaller heat transfer coefficients for the mixtures. However, as depicted by Sardesai *et al.* [13], the determination of the composition shift is too complex for design calculation. Therefore, Sardesai *et al.* [13] suggest that $T_w - T_{buuble,i}$ should be used for engineering applications.

The determination of the inside heat transfer coefficient, h_i, requires knowledge of the outside heat transfer coefficient, h_o. This was accomplished by means of separate water-to-water tests on the same apparatus, with subsequent Wilson-plot analyses yielding the individual heat transfer coefficient relationships. The vapour quality entering the test section (x_{in}) was calculated from the energy balance of the preheater and the quality change in the test section and is given by the energy balance:

$$\Delta x = \frac{\dot{Q}}{m_r i_{fg}} \tag{3}$$

and the average quality in the test section is given by

$$x_{ave} = x_{\epsilon} + \frac{\Delta x}{2}. \tag{4}$$

PRESSURE DROP DATA REDUCTION

The pressure drop data are obtained in two ways, one with heat addition and the other for adiabatic flow. For evaporation flows, additional pressure drop due to acceleration, ΔP_a, must be included. The frictional pressure gradient data were analyzed using the concept of the two-phase multiplier. Because the acceleration pressure gradient, ΔP_a, can be neglected, adiabatic experiments provide more accurate calculation of the frictional multiplier. The multiplier is defined by

$$\phi_l^2 = \frac{\dfrac{dP_f}{dz}}{\dfrac{dP_{f,l}}{dz}}, \tag{5}$$

where dP_f is the measured two-phase frictional pressure gradient and $dP_{f,l}$ is the frictional pressure gradient corresponding to the cases of liquid flowing alone in the channel. The multiplier typically plotted versus vapour quality x or the Martinelli parameter X, where

$$X = \frac{\sqrt{\left(\dfrac{dP_{f,l}}{dz}\right)}}{\left(\dfrac{dP_{f,v}}{dz}\right)}. \tag{6}$$

To obtain the Martinelli parameter X, it is necessary to obtain the friction factor of the single-phase liquid flow. Figure 3 shows f_l versus Re_{Di} for the tested tubes. The base line is the Blasius friction factor equation ($0.079Re_{Di}^{-0.25}$). The lowest experimental Re_{Di} is approximately 2300. The friction factors for the smooth and micro-fin tubes are approximately 9 and 45% higher, respectively, than those predicted by the Blasius equation. The curve-fitted equations are also depicted in Fig. 3.

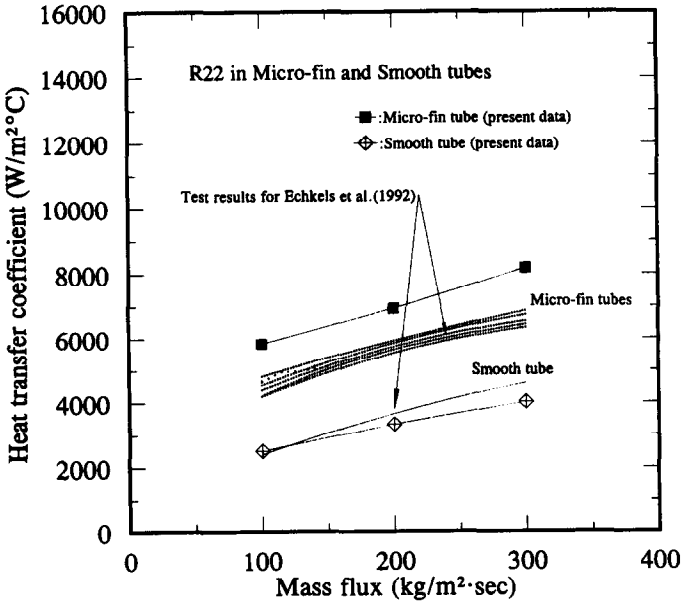

Fig. 4. Comparison of the average heat transfer coefficients with Echkels and Pate's data (R22).

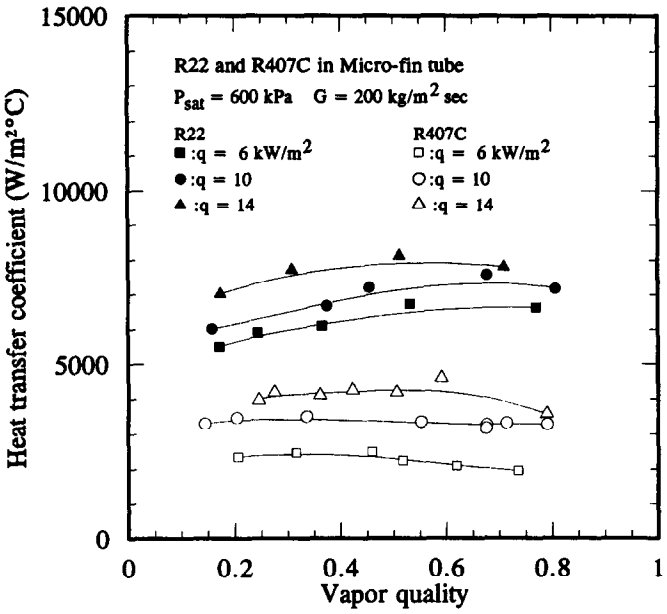

Fig. 5. Effect of heat flux on the evaporating heat transfer coefficient.

RESULTS AND DISCUSSION

Figure 4 shows the heat transfer results for the pure refrigerant (R22) for both micro-fin and smooth tube as compared to the data of Eckels and Pate [14]. Comparing the average heat transfer coefficients for their five different configuration micro-fin tubes (all with 9.52 mm nominal diameter) indicated that some differences exist in the performances of the fin designs. However, the differences are relatively small, as shown in Fig. 4. The present test micro-fin tube gives 15% higher heat transfer coefficients as compared to the Eckels and Pate [14] data. The reasons for this phenomenon are two-fold. Firstly, the heat fluxes tested by Eckels and Pate [14] (approximately 4~8 kW/m^2) were somewhat lower than those of the present investigation (6~14 kW/m^2). It is known that the two-phase boiling heat transfer coefficients are strongly dependent upon heat flux. For instance, a close examination of the micro-fin data by Chiang [6] indicates that the boiling heat transfer coefficient is approximately proportional to $q^{0.25}$ (also use R22 as the working medium). Secondly, the tested micro-fin tubes used by Eckels and Pate [14] were expanded tubes. This indicates that the tube diameter was larger than its original nominal tube, namely $D_o > 9.52$ mm. For a practical mechanically expanded tube, $D_o \approx 10$ mm. As illustrated by Tsuchida *et al.* [15], the evaporation heat transfer coefficients increase with the decrease of tube diameter. As a result, higher heat transfer coefficients may be encountered for the present test micro-fin tube.

Figure 5 shows the variation of heat transfer coefficient versus vapour quality with a fixed mass flux and varying heat flux ($G = 200$ kg/m^2·s, $P = 600$ kPa, $q = 6$, 10 and 14 kW/m^2, respectively). As expected, the heat transfer coefficients increase with the heat flux, and our measurements show that the heat transfer coefficient for R22 is approximately proportional to $q^{0.24}$. The experimental data for pure refrigerant, R22, show a mild increase of heat transfer coefficient with the vapour quality. However, the evaporation heat transfer coefficients of R407C are relatively independent of vapour quality. Actually, for lower mass flux ($G = 100$ kg/m^2·s), the heat transfer coefficients decrease slowly with the increase of vapour quality. The results are similar to the data of R402A and R404A conducted by Kattan *et al.* [16]. Note that R402A and R404A are also mixtures. The experimental data for the pure refrigerant, R22, do not reveal this kind of decreasing behaviour. The possible reasons for this phenomenon are two-fold. Firstly, Kattan *et al.* [17] show that the flow pattern of the mixtures 402A and 404A are in the stratified regime, even though their liquid Froude numbers were 13 and 16 times above the recommended threshold values. This may explain the different heat transfer characteristics for R407C. Secondly, as addressed previously, the driving

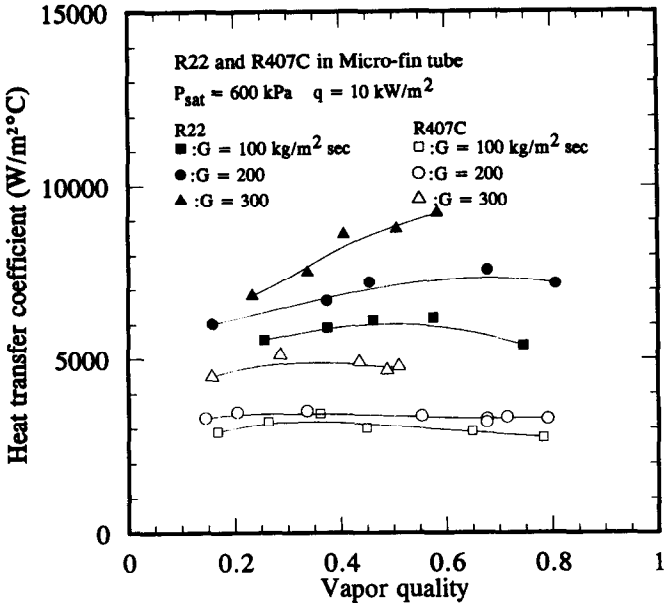

Fig. 6. Effect of mass flux on the evaporating heat transfer coefficient.

potential is based on the initial composition of R407C and this larger driving potential may result in smaller heat transfer coefficients.

The experimental data also indicate that the heat transfer coefficients of R407C are 50~80% less than those of R22. The experimental data are consistent with the test results by Sumida *et al.* [18]. Their data indicate that the heat transfer coefficients for R407C are 30–40% lower than those of R22. Note that their effective temperature potentials are based upon measured refrigerant temperature, which is close to $T_w - T_{bubble,x}$, and is less than the inlet driving potential, $T_w - T_{bubble,i}$. Therefore, a much larger reduction of heat transfer coefficients as compared to R22 is likely when $T_w - T_{bubble,i}$ is used as the driving potential in the present study.

Figure 6 shows the effect of mass flux at fixed heat flux. This figure shows a strong effect of mass flux on the heat transfer performance. For a prescribed heat flux (q = 10 kW/m^2), the heat transfer

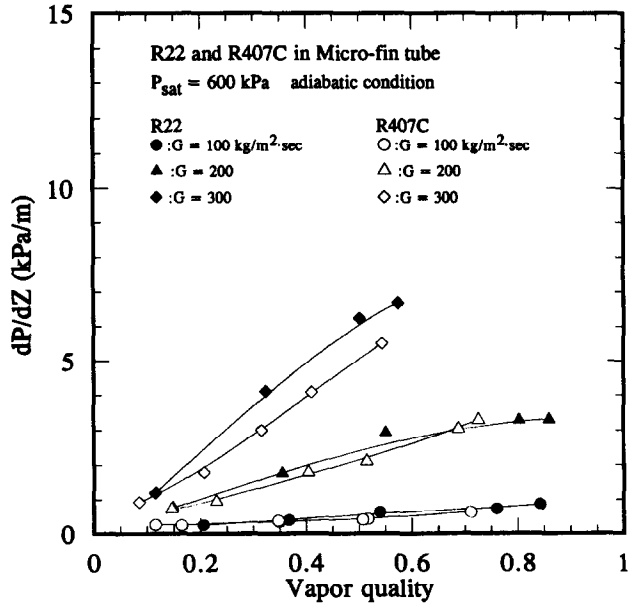

Fig. 7. Pressure drop gradient vs vapour quality at various mass flux (adiabatic conditions).

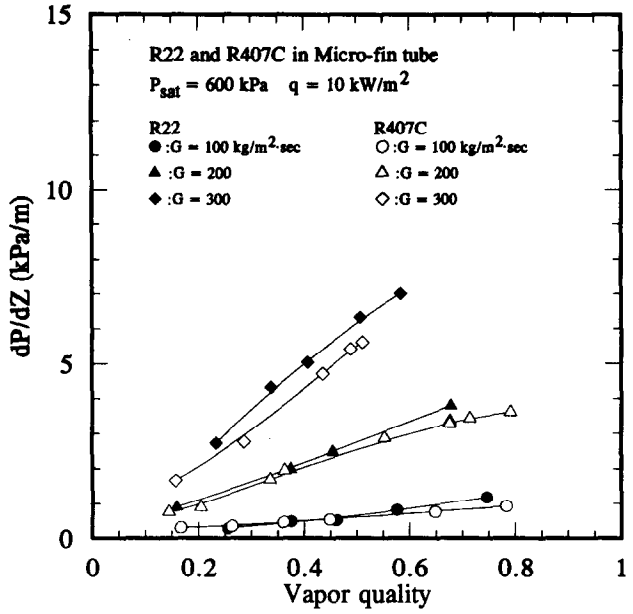

Fig. 8. Pressure drop gradient vs vapour quality at various mass flux with heat addition.

coefficients increase with the mass flux. This result is similar to the previous studies, as depicted by Echkels and Pate [14]. On examination of the R22 data points using the flow pattern map proposed by Taitel and Dukler [19], one can find that, for lower mass flux $G = 100$ kg/m^2·s, the flow pattern for the tested data are in the stratified wavy region or close to the margin between the annular and stratified flow region. As a result, a smaller heat transfer coefficient is expected and no detectable increase of heat transfer coefficients versus vapour quality is found. For a higher mass flux, $G = 300$ kg/m^2·s, the flow pattern for the test data changes from the boundary of intermittent flow and annular flow pattern to annular flow pattern as vapour quality increases. As a result, the heat transfer coefficients increase with the vapour quality. The effects of mass flux on the level off phenomena of heat transfer coefficient are similar for both R22 and R407C. Namely, the local maxima increase with the mass flux. However, R407C does not show a noticeable increase of heat transfer coefficient versus vapour quality as mass flux increases. Actually, all of the R407C data reveal this phenomena. Similar test results for the mixtures R402A and R404A are reported by Kattan *et al.* [16]. Kattan *et al.* [20] suggest the VDI flow pattern map (a modified Taitel–Dukler flow pattern map given in VDI-Warmeatlas [21]) is used to predict the new refrigerants. By examination of the R407C data using the VDI flow pattern map, we found that most of the experimental data are in the wavy flow regime. Accordingly, R407C data show no detectable increase of heat transfer coefficients versus vapour quality. The experimental data suggest that the pure refrigerants R22 and R407C should use different flow pattern maps.

For adiabatic conditions, the pressure drop data for the test tube are shown in Fig. 7. The pressure drop (expressed as $\Delta p/L$, i.e. pressure drop per unit length) increases significantly with the mass flux and with quality. As seen in the figure, the increasing rate of frictional gradients increase with mass flux G. For a given quality, the pressure gradient is approximately proportional to $G^{2.45}$ for both of the refrigerants. However, the experimental data indicate that the pressure gradients are considerably lower for R407C. Typically, a 45% reduction in the pressure gradients was observed for R407C. Again, the reduction in pressure gradients may be attributed to the flow pattern difference between the tested refrigerants. As addressed previously, mixtures are likely in the stratified regime, even though their liquid Froude numbers were 13 and 16 times above the recommended threshold values. This may explain the significant reduction in both of the heat transfer and pressure gradients. Figure 8 shows the pressure drop gradient data for the test tubes with heat addition conditions ($q = 10$ kW/m^2). As seen, approximately a 10% increase of pressure drop with heat addition conditions were shown. This indicates that the acceleration pressure loss is approximately 10% of the total pressure drop.

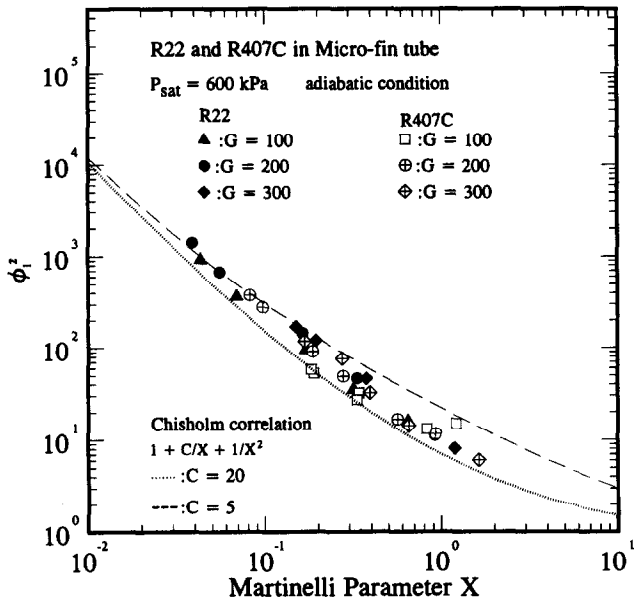

Fig. 9. Frictional multiplier vs Martinelli parameter for the experimental data.

For smooth, circular tubes, one may correlate the friction data from $\phi_l^2 = \phi_l^2(X)$. As proposed by Chisholm [22]:

$$\phi_l^2 = 1 + \frac{C}{X} + \frac{1}{X^2}, \tag{7}$$

where X is the Martinelli parameter, and is given by equation (6), for smooth tubes, the constant C ranges from 5 to 20, depending on whether the liquid and vapour phases are laminar or turbulent. The constant C is dependent on other things, like physical properties of the mixture. In particular, the C factor can be adjusted to give a best fit to a given set of data. Figure 9 shows the measured data plotted in the form ϕ_l^2 versus X_{tt} for both R22 and R407C, respectively. Also shown in the

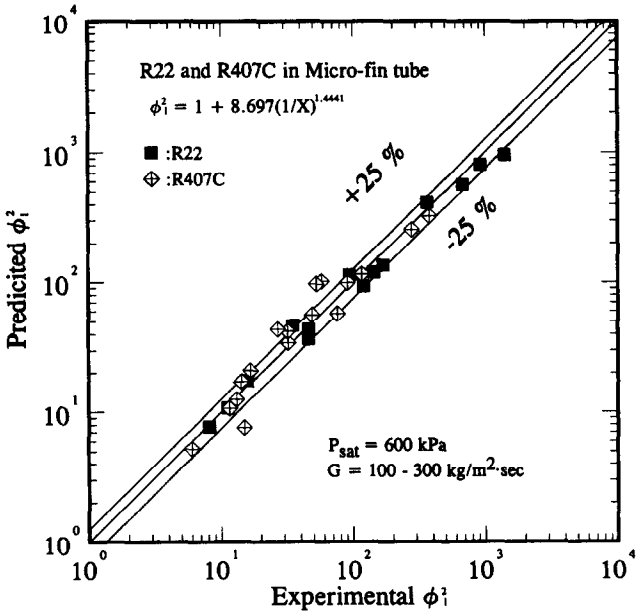

Fig. 10. Comparison of the experimental frictional multiplier with the present correlation for both R22 and R407C.

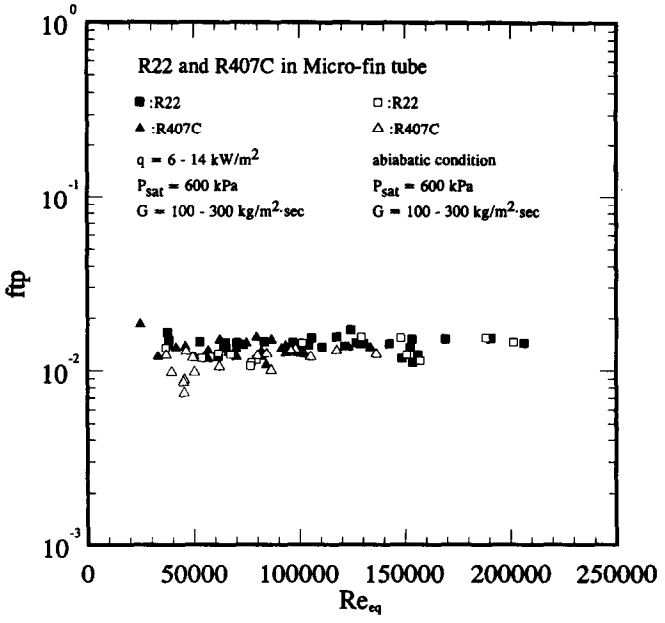

Fig. 11. Two-phase flow friction factors for both R22 and R407C.

figure are the values predicted by equation (7) for $C = 5$ and 20. Our data shows that C is between 5 and 20. As seen, the experimental data deviate from a constant value. The reason for this deviation is that the Chisholm correlation was based on the data mainly from relatively large diameter and larger mass fluxes. Wambsganss *et al.*'s [23] data also suggest a variable C with various mass fluxes. Their experimental data indicate that a constant value of $C = 21$ would provide good agreement for the higher mass fluxes data ($G > 400$ kg/m^2·s) and a C value less than 5 is encountered when mass flux is equal to 50 kg/m^2·s. Therefore, the use of a constant value of C over the entire mass flux would provide a rather poor accuracy. Therefore, the present ϕ_l^2 can be correlated as

$$\phi_l^2 = 1.0 + 7.757\left(\frac{1}{X_{tt}}\right)^{1.493}. \tag{8}$$

As seen in Fig. 10, 86% of the experimental data were correlated within 25%, and equation (8) is applicable to both R22 and R407C.

An alternative approach to reduce the two-phase friction data is to introduce the two-phase friction factor f_{tp}. Using a mean two-phase viscosity, $\bar{\mu}$ in the normal friction factor relationship, the two-phase friction factors can be expressed as

$$\left(\frac{dP}{dz}\right)_{\text{Two-phase pressure drop}} = \frac{2f_{tp}G^2\bar{v}}{D_i} \tag{9}$$

and

$$\bar{v} = xv_v + (1 - x)v_l \tag{10}$$

$$\bar{\mu} = \bar{\rho}(xv_v\mu_v + (1 - x)v_l\mu_l) \tag{11}$$

$$\text{Re}_{eq} = \frac{GD_i}{\bar{\mu}}. \tag{12}$$

The mean two-phase viscosity is taken from Dukler *et al.* [24]. Figure 11 shows the two-phase friction factors defined by equation (9) plotted against Re_{eq} for both R22 and R407C. The figure shows a very small dependence of the friction factor on the Reynolds number. Similar results were reported by Yang and Webb [25] in their rectangular conduit. Note that Yang and Webb use

hydraulic diameter in correlating their friction data, instead of tube diameter. The experimental data presented here suggest $f_{tp} \approx 0.0127$ for both R22 and R407C.

CONCLUSIONS

An experimental study of evaporation in a 9.52 mm micro-fin tube with R22 and R407C refrigerant is presented in this study. The experimental data were taken at an evaporation pressure of 600 kPa, the range of mass flux is between 100 to 300 kg/m^2·s and the heat flux varies from 6 to 14 kW/m^2. Data are presented in the form of locally length-averaged heat transfer coefficients and frictional pressure gradients. The effect of heat flux, mass flux and pressure on the heat transfer coefficient are reported in the present investigation. The heat transfer coefficient increases with heat flux and mass flux for R22, and the reduction of heat transfer coefficients for R407C as compared to R22 are approximately 50~80%. The reduction in the pressure gradient for R407C is approximately 45% compared to R22. The reduction in both the heat transfer coefficients and friction gradients may be attributed to the difference in flow pattern for the pure refrigerant and the mixture and the definition of the temperature driving potential of the R407C mixtures. Meanwhile, it is suggested that the use of flow pattern maps should be different for pure refrigerant and the mixtures.

Acknowledgements—The authors would like to express gratitude for the Energy R & D foundation funding from the Energy Commission of the Ministry of Economic Affairs to support this research work. The authors are indebted to Mr Klaus Menze at Wieland-Werke AG for providing the ripple fin tubes.

REFERENCES

1. R. L. Webb, *Principles of Enhanced Heat Transfer*, Chapter 1. Wiley Interscience, New York (1994).
2. J. C. Khanara, M. B. Pate and A. E. Bergles, Augumented in-tube evaporation of refrigerant 113. *Boiling and Condensation in Heat Transfer Equipment*, HTD-85, pp. 21–30 (1987).
3. M. Ito, H. Kimura and T. Senshu, Development of high-efficiency air-cooled heat exchangers. *Hitachi Review* **26,** 323–326 (1977).
4. M. Ito and H. Kimura, Boiling heat transfer and pressure drop in internal spiral-grooved tubes. *Bull. JSME* **22,** 1251–1257 (1979).
5. L. M. Schlager, A. E. Bergles and M. B. Pate, Heat transfer and pressure drop during evaporation and condensation of R-22 in horizontal micro-fin tubes. *Int. J. Refrig.* **12,** 6–14 (1988).
6. R. Chiang, Heat transfer and pressure drop during evaporation and condensation of refrigerant-22 in a 7.5 mm diameter axial and helical grooved tubes. *AIChE Symp. Series* **89**, 205–210 (1993).
7. S. J. Eckels and M. B. Pate, In-tube evaporation and condensation of refrigerant-lubricant mixtures of HFC-134a and CFC-12. *ASHRAE Trans.* **97,** 62–70 (1991).
8. H. Ross and R. Radermacher, Horizontal flow boiling of pure and mixed refrigerants. *Int. J. Heat Mass Transfer* **30**(5), 979–992 (1987).
9. D. S. Jung and R. Radermacher, Horizontal flow boiling heat transfer with refrigerant mixtures of R22/R114. *Int J. Heat Mass Transfer* **32**(1), 131–145 (1989).
10. S. P. Wang and J. C. Chato, Review of recent research on heat transfer with mixtures—Part 2: boiling and evaporation. Presented in ASHRAE Winter Meeting, paper number CH-95-23-3 (1995).
11. NIST 1994. REFPROP, Gaithersburg, MD. National Institute of Standards and Technology (1994).
12. R. J. Moffat, Describing the uncertainties in experimental results. *Experimental Thermal and Fluid Science* **1,** 3–17 (1988).
13. R. G. Sardesai, R. A. W. Shock and D. Butterworth, Heat and mass transfer in multicomponent condensation and boiling. *Heat Transfer Engng.* **3**(3), 104–114 (1982).
14. S. J. Eckels and M. B. Pate, Evaporation heat transfer coefficients for R-22 in micro-fin tubes of different configuration. *Enhanced Heat Transfer*, HTD-202, ASME, pp. 117–125 (1992).
15. T. Tsuchida, K. Yasuda, M. Hori and T. Otani, Internal heat transfer characteristics and workability of 'THERMOFIN' tubes. *Hitachi Cable Review*, No. 12, pp. 59–64 (1993).
16. N. Kattan, J. R. Thome and F. Favrat, R-502 and two near-azeotropic alternatives: part I. In-tube flow boiling tests. Presented at ASHRAE Winter Meeting, paper number CH-95-12-3 (1995a).
17. N. Kattan, J. R. Thome and F. Favrat, R-502 and two near-azeotropic alternatives: part II. Two-phase flow patterns. Presented at ASHRAE Winter Meeting, paper number CH-95-14-3 (1995b).
18. T. Hiruto, M. Todakazu, K. Y. Okuyama and K. Torikoshi, Investigation of heat transfer and friction characteristics of Nonazeotropic refrigerant of HFC-32/125/134a (R407C). *Proc. 29th Japanese Joint Conf. on Air-conditioning and Refrigeration (Tokyo)*, pp. 69–72 (1995) (in Japanese).
19. Y. Taitel and A. E. Dulker, A model for predicting flow regime transitions in horizontal and near horizontal gas–liquid flow. *AIChE J.* **22,** 47–55 (1976).
20. N. Kattan, J. R. Thome and F. Favrat, Measurement and prediction of two-phase flow patterns for new refrigerants inside horizontal tubes. Presented at ASHRAE Summer Meeting, paper number SD-95-17-4 (1995c).
21. VDI-Warmeatlas. Heat Transfer to boiling saturated liquids. *VDI Heat Atlas*, Chapter Hbb1. VDI, Dusseldorf, Germany (1993).

22. D. Chisholm, A theoretical basis for the Lockhart–Martinelli correlation for two-phase flow. *Int. J. Heat Mass Transfer* **10,** 1767–1778 (1967).
23. M. W. Wambsganss, J. A. Jendrzejcyk, D. M. France and N. T. Obot, Friction pressure gradients in two-phase flow in a small horizontal rectangular channel. *Exp. Thermal Fluid Sci.* **5,** 40–56 (1992).
24. A. E. Dulker, M. Wicks and R. G. Cleveland, Pressure drop and hold up in two-phase flow. Part A. A comparison of existing correlations. Part B. An approach through similarity analysis. *AIChE J.* **10,** 38–51 (1964).
25. C. Y. Yang and R. L. Webb, Condensation of R-12 in small hydraulic diameter extruded aluminum tubes with and without micro-fins. *Int. J. Heat Mass Transfer* (accepted).